Nano Research

Open Access

Research Article

Suppression of chlorine-related side reactions via spin control for sustainable seawater electrolysis

Jisi Li[1], Ruguang wang[1], Jiaxin Guo[1,2], Quanlu Wang[1], Zheng Lv[1], Ruize Ma[1], and Tao Ling[1]✉

[1] School of Materials Science and Engineering, Tianjin University, Tianjin 300072, China
[2] Institute of Atomic Manufacturing, Beihang University, Beijing 100191, China

Cite this article: Nano Research, **2026**, *19*, 94908738. https://doi.org/10.26599/NR.2026.94908738

ABSTRACT: Seawater electrolysis offers a promising route to green hydrogen production by utilizing abundant seawater resources, yet its commercial viability is hindered by chlorine-related side reactions that cause corrosion and reduce efficiency. Current strategies mainly employing anion-enriched layers to repel chloride ions face challenges, as these pre-designed structures may not dynamically maintain selective exclusion under varying operational potentials. Here, we propose a fundamentally different approach based on spin-mediated selectivity and employ a series of spinel oxides with varying magnetic properties to elucidate the correlation between spin regulation, anodic reaction selectivity, and electrolysis stability. We demonstrate that ferromagnetic catalysts intrinsically strengthen hydroxyl adsorption while suppressing chloride binding, thereby favoring oxygen evolution over competing chlorine chemistry. Mechanistically, spin alignment facilitates the formation of triplet oxygen and inhibits chlorinated byproducts. Benefiting from such intrinsic selectivity, catalysts with stronger ferromagnetism exhibit superior operational stability in seawater electrolysis, maintaining stable performance for 120 h in an anion exchange membrane water electrolyzer. This work establishes spin regulation as a complementary strategy for designing highly selective and durable electrocatalysts, offering a new pathway to address the limitations of conventional protection layers in practical seawater splitting.

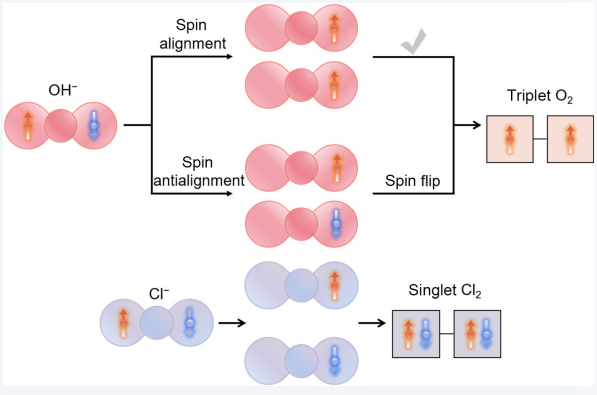

KEYWORDS: spin control, seawater electrolysis, oxygen evolution reaction (OER), chlorine chemistry

1 Introduction

As an important supplement to traditional pure water electrolysis for hydrogen production, seawater electrolysis provides a breakthrough solution for building a global green hydrogen energy system [1, 2]. Compared with conventional technology that relies on high-purity freshwater as feedstock, seawater electrolysis directly employs earth-abundant seawater resources. This alleviates water resource constraints and lowers water treatment costs [3, 4]. More attractively, seawater electrolysis can be integrated with offshore/coastal renewable energy, thus achieving the full resource-production-application chain of hydrogen energy through on-site utilization [5, 6]. Unfortunately, the complex composition of seawater poses a key challenge for the commercial application of seawater electrolysis technology—especially the corrosion problem caused by the high concentration of chloride ions (Cl^-, ~ 0.5 M), which is closely related to the long-term operational stability and economic feasibility of the system [7–11].

During electrolysis, Cl^- in seawater undergoes the chlorine evolution/oxidation reaction (ClER/ClOR, under acidic/alkaline conditions, respectively), which competes with the oxygen evolution reaction (OER) at the anode [12–14]. This not only reduces electrolysis efficiency but also leads to severe catalyst/electrolyzer corrosion caused by chlorine-related by-products. To address this issue, current research usually adjusts the pH value of seawater above 13 to maximize the thermodynamic potential difference between ClOR and OER, thereby partially suppressing chlorine-related side reactions [4, 15]. Building on this, a widely adopted strategy involves constructing an anion-enriched layer on the catalyst surface to inhibit Cl^- adsorption through electrostatic repulsion [7, 9, 10, 16, 17]. Although significant

Received: March 11, 2026; **Revised:** April 12, 2026
Accepted: April 15, 2026

✉Address correspondence to lingt04@tju.edu.cn

progress has been made, the anion-enriched layer and interface interactions change dynamically with the applied potential, making it difficult for pre-designed structures to consistently block Cl^- throughout the electrolysis process [18]. Furthermore, whether the anion-enriched layer can selectively allow the passage of alkaline OER reactants (OH^-) while repelling Cl^- remains debated [12, 19]. Therefore, developing catalysts with intrinsic selectivity to fundamentally suppress chlorine-related side reactions remains a critical objective.

In recent years, spin effects [20–25] in electrochemical reactions have emerged as a new approach to modulate electrocatalytic processes. For OER, which involves the generation of triplet oxygen, the non-conservation of electron spin significantly increases the reaction energy barrier and causes additional energy loss [26, 27]. In contrast, spin-selective electron transfer pathways constructed via intrinsic chirality/magnetic properties or external field regulation can accelerate spin-dependent OER kinetics [28–33]. Notably, spin control provides an effective strategy for tuning selectivity in complex competitive electrochemical systems, such as eliminating singlet hydrogen peroxide formation during water splitting [22, 34]. Given the distinct spin characteristics of electron transfer in OER versus ClER/ClOR [18]—namely, that OER involves the spin-forbidden formation of triplet oxygen, whereas ClER/ClOR only involve spin-allowed singlet-state transformations—leveraging the spin effects of catalysts enables spin-selective promotion of OER and simultaneous suppression of chlorine-mediated side reactions during seawater electrolysis. Nevertheless, research on rationally designing intrinsically selective catalysts for seawater electrolysis via spin regulation remains scarce, and the underlying mechanisms require further systematic elucidation.

In this work, a series of spinel oxides with different magnetic properties were used as model materials to reveal the mechanism by which spin control enhances the efficiency and stability of seawater electrolysis. We found a positive correlation between magnetism and the binding strength of the catalysts to OH^-, while a negative correlation exists with Cl^-—a trend that leads to differences in the anodic selectivity of seawater electrolysis. Combined with the molecular orbital model, we uncovered the physical origin that ferromagnetism essentially promotes the formation of triplet oxygen molecules and inhibits singlet chlorine products by controlling spin alignment, which was further verified by external magnetic field tests. Ultimately, due to the improved selectivity, catalysts with stronger ferromagnetism exhibited higher stability in seawater electrolysis and could operate stably for 120 h in an anion exchange membrane water electrolyzer (AEMWE).

2 Results and discussion

2.1 Construction of spinel ferrite systems with different magnetic properties

Earth-abundant spinel oxides are typical non-noble metal electrocatalysts for OER, and their tunable compositions and interactions make them excellent model materials for investigating structure-performance relationships [35, 36]. To systematically explore the underlying mechanism of spin/magnetic effects in regulating seawater electrolysis performance, a series of spinel ferrites—denoted by the general formula MFe_2O_4 (where M refers to Co^{2+}, Ni^{2+}, Mg^{2+}, or Zn^{2+} and Fe denotes Fe^{3+})—featuring both octahedral and tetrahedral coordination sites were selected as model materials in this work (Fig. 1(a)). These samples were subsequently synthesized by a unified hydrothermal procedure, with their structural consistency validated by X-ray diffraction (XRD), energy dispersive spectroscopy (EDS), and X-ray photoelectron spectroscopy (XPS) (Figs. S1–S3 in the Electronic Supplementary Material (ESM)). As shown in Fig. 1(b), all diffraction peaks of the four samples can be well indexed to the cubic spinel structure with the $Fd\bar{3}m$ space group, verifying an identical crystal framework across all samples and ensuring their comparability for subsequent tests.

With the four comparable MFe_2O_4 model systems successfully constructed, their magnetic properties were systematically characterized using a physical property measurement system (PPMS). The magnetic hysteresis loops clearly reflect the distinct magnetic behaviors of the four samples (Fig. 1(c)): $CoFe_2O_4$, $NiFe_2O_4$, and $MgFe_2O_4$ exhibit strong, moderate, and very weak ferromagnetic or ferrimagnetic characteristics, respectively, among which $CoFe_2O_4$ shows a distinct hysteresis loop with obvious coercivity and remanence; in sharp contrast, $ZnFe_2O_4$ possesses extremely low magnetic susceptibility, indicating antiferromagnetic or paramagnetic behavior [28]. Note that the magnetic differences arise from the distinct cation distributions between tetrahedral and octahedral sites in the spinel lattice: Co^{2+} and Ni^{2+} prefer octahedral sites while Mg^{2+} and Zn^{2+} prefer tetrahedral sites. To quantitatively evaluate the relative magnetic strength of the four samples, the magnetization at a magnetic field of 10,000 Oe (denoted as M_{10000}, consistent with the field intensity applied in external magnetic field experiments, discussed later) was extracted from the hysteresis loops (Fig. 1(c), inset). The results show that the M_{10000} values follow the order of $CoFe_2O_4$ > $NiFe_2O_4$ > $MgFe_2O_4$ > $ZnFe_2O_4$, indicating a gradual decrease in magnetic strength among the four spinel ferrite samples. This distinct difference in magnetic properties, combined with their structural consistency, provides an ideal platform for exploring the regulatory effect of spin/magnetism on seawater electrolysis electrocatalysis.

2.2 Investigation on *OH binding strength and OER activity of spinel ferrites

Building on the magnetic property characterization of spinel ferrites, further investigations focused on the correlation between their spin/magnetic effects and electrocatalytic performance for seawater electrolysis. It is well established in previous literature [23, 37] that ferromagnetic oxides can promote the delocalization of parallel-spin electrons via spin alignment, which is closely associated with strong metal–oxygen hybridization (Fig. 2(a)). This enhanced metal–oxygen hybridization is critical for strengthening the adsorption capacity of metal sites toward hydroxyl species (*OH) [38–40], laying a solid foundation for regulating electrocatalytic behaviors.

To quantitatively clarify the relationship between magnetic strength and *OH binding strength, methanol molecular probing experiments [41] were conducted (Fig. S4 in the ESM). As depicted in Fig. 2(b), the charge associated with *OH coverage (denoted as Q_{*OH}) clearly reveals that *OH binding strength follows the order of $CoFe_2O_4$ > $NiFe_2O_4$ > $MgFe_2O_4$ > $ZnFe_2O_4$. Notably, this order is consistent with the sequence of their magnetization at 10,000 Oe (M_{10000}), confirming a positive correlation between the magnetic strength of spinel ferrites and their *OH binding strength (Fig. S5 in the ESM). This positive correlation arises from enhanced

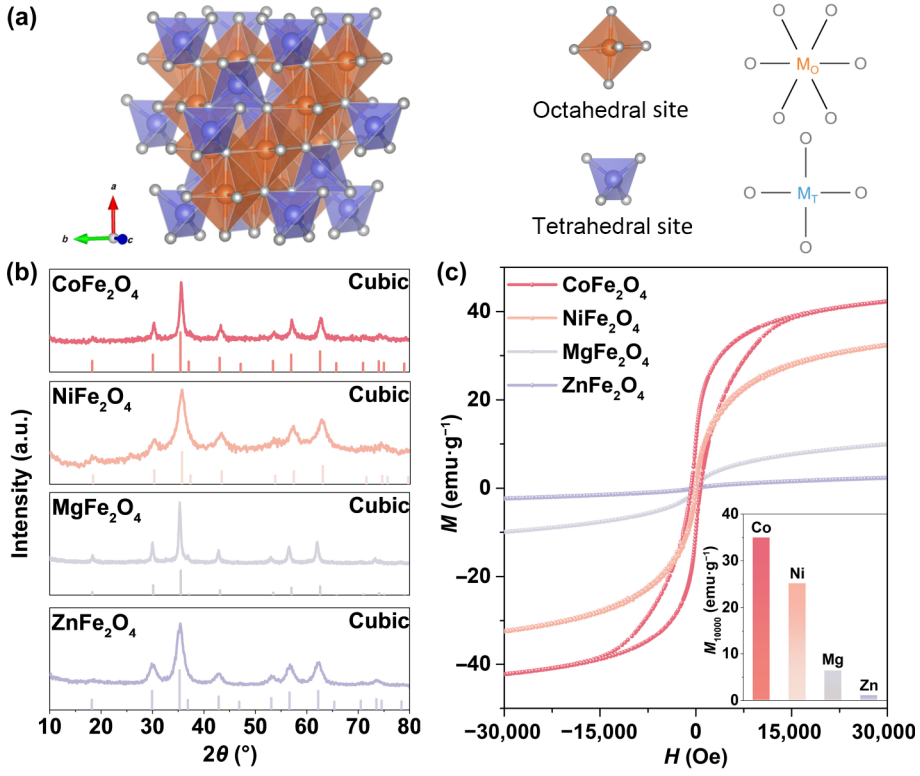

Figure 1 Structural and magnetic characterizations of as-prepared MFe_2O_4 spinel ferrites. (a) Schematic illustration of the typical crystal structure of spinel ferrites, featuring distinct tetrahedral and octahedral coordination sites for metal cations. (b) XRD patterns of the as-prepared MFe_2O_4 samples. (c) Room-temperature magnetic hysteresis loops of the as-prepared MFe_2O_4 samples; inset: comparison of magnetization at 10,000 Oe (M_{10000}) for the MFe_2O_4 samples.

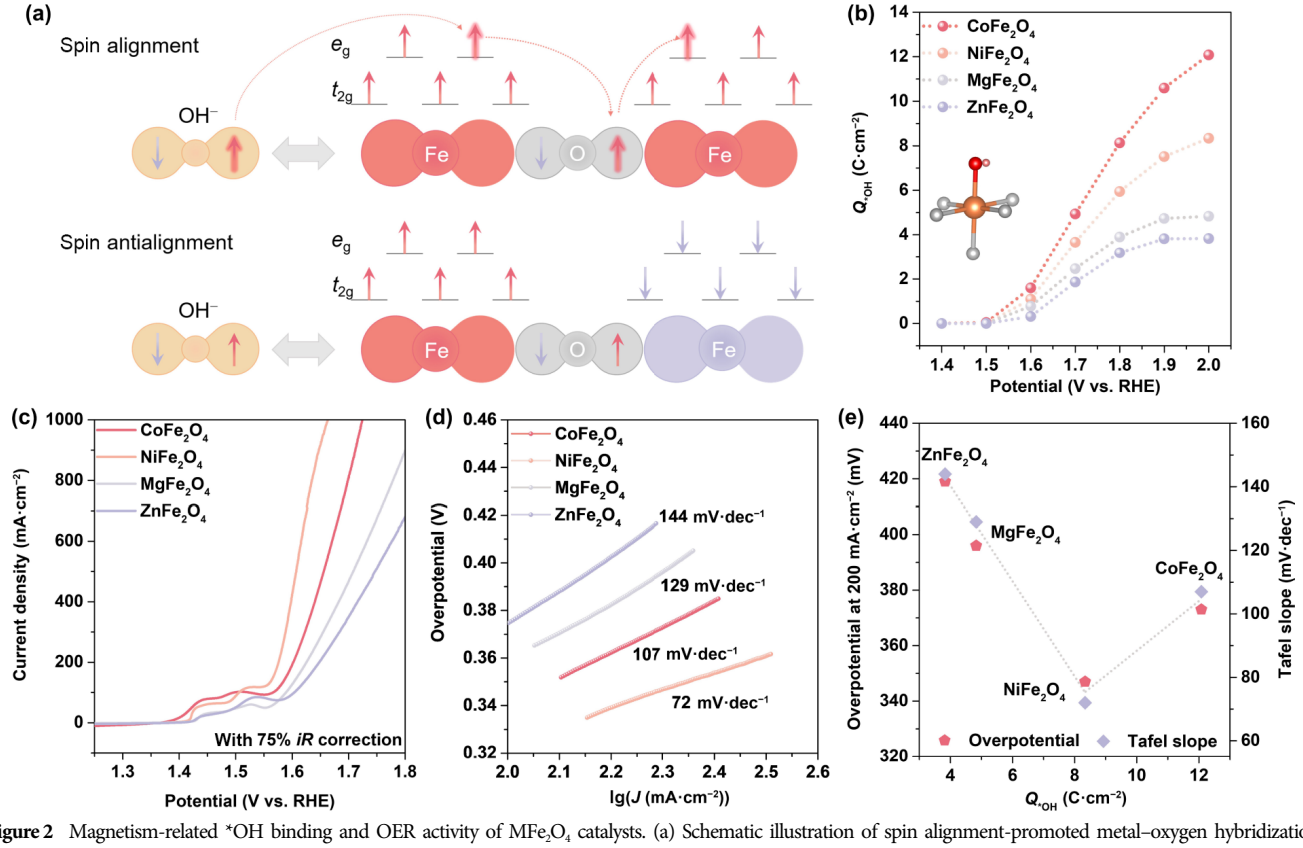

Figure 2 Magnetism-related *OH binding and OER activity of MFe_2O_4 catalysts. (a) Schematic illustration of spin alignment-promoted metal–oxygen hybridization, which enhances the OH^- adsorption on the catalyst surface. (b) Comparison of Q_{OH} for the MFe_2O_4 catalysts, acquired from methanol molecular probing experiments. (c) LSV curves of the MFe_2O_4 catalysts in alkalized seawater at a scan rate of 5 mV·s^{-1} with 75% *iR* correction. (d) Corresponding Tafel plots derived from the LSV curves in (c). (e) Inverted volcano plot of OER overpotential and Tafel slope versus Q_{OH}.

ferromagnetism, which is associated with strong metal–oxygen hybridization, thereby strengthening the interaction between active sites and *OH intermediates.

On this basis, electrochemical tests were carried out to evaluate their activity. The catalysts were *in-situ* grown on nickel foam (NF) substrates, and all tests were performed in alkalized seawater (1 M NaOH + seawater, Fig. S6 in the ESM). Linear sweep voltammetry (LSV) curves indicate that the overpotentials of the four samples follow the order of $NiFe_2O_4$ < $CoFe_2O_4$ < $MgFe_2O_4$ < $ZnFe_2O_4$ (Fig. 2(c) and Fig. S7 in the ESM), with the Tafel slopes showing the same trend (Fig. 2(d)). Note that we have eliminated the influence caused by the difference in intrinsic electronic conductivity of the four catalysts through electrochemical impedance spectroscopy (EIS) measurements (Fig. S8 in the ESM). These results indicate that $NiFe_2O_4$ has the optimal OER activity, followed by $CoFe_2O_4$ and then $MgFe_2O_4$, while $ZnFe_2O_4$ shows relatively poor performance.

It should be noted that the OER activity of the four spinel ferrites is not in a simple linear relationship with their magnetic strength (M_{10000}). A brief plot of OER activity indicators (overpotential and Tafel slope) against Q_{*OH} shows a typical inverted volcano curve (Fig. 2(e)), indicating that $NiFe_2O_4$ with relatively strong magnetism has the most appropriate *OH binding energy for OER catalysis, while the most magnetic $CoFe_2O_4$ has a slightly higher binding energy. Overall, strong magnetism does not necessarily correspond to the highest OER activity; instead, magnetism regulates OER activity through *OH binding strength rather than a direct linear correlation (Fig. S9 in the ESM).

2.3 Exploration on chlorine chemistry of spinel ferrites

At the seawater electrolysis anode, Cl^- competes with OH^- for adsorption sites, and ClOR competes with OER under alkaline conditions, which corrode the catalyst and reduce the stability of the electrolysis system [4, 15]. Clarifying the chlorine chemistry of the four spinel ferrites is therefore essential. Firstly, to systematically examine the Cl^- adsorption behavior on the surface of the four spinel ferrites after long-term seawater electrolysis, XPS tests were performed on the catalysts after 10 h of electrolysis at a constant current density of 0.5 A·cm^{-2} (Fig. 3(a)). From the Cl 2p XPS spectra, distinct differences in Cl^- adsorption among the four samples are clearly observed: $ZnFe_2O_4$ exhibits obvious Cl 2p characteristic peaks at around 198 eV (Cl $2p_{3/2}$) and 200 eV (Cl $2p_{1/2}$), while the Cl 2p peaks of $CoFe_2O_4$ are barely detectable. This trend—strongest Cl^- adsorption on $ZnFe_2O_4$ and weakest on $CoFe_2O_4$—extends to all four samples, following a clear order: $CoFe_2O_4$ < $NiFe_2O_4$ < $MgFe_2O_4$ < $ZnFe_2O_4$. Notably, this order is opposite to the *OH adsorption behavior of the four samples and exhibits a negative correlation with their magnetic strength (M_{10000}, Fig. S10 in the ESM).

This phenomenon can be explained by the competitive adsorption mechanism on catalyst active sites. Both OH^- and Cl^-

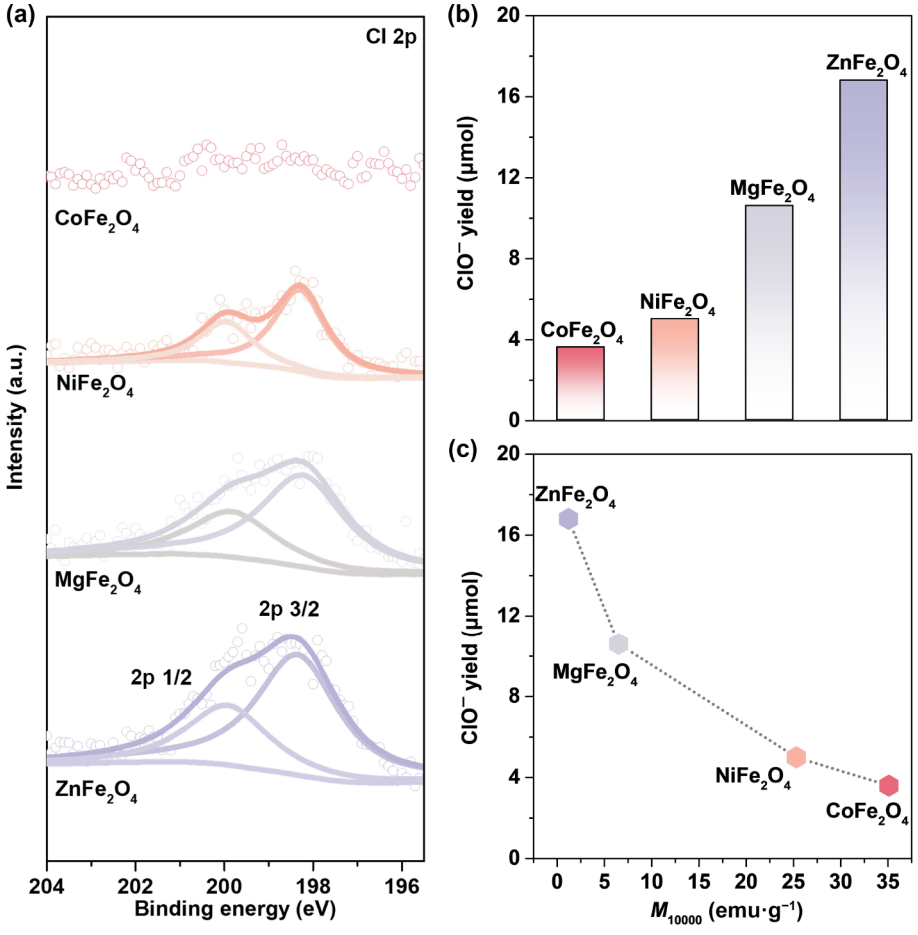

Figure 3 Magnetism-related chlorine chemistry of MFe_2O_4 catalysts. (a) Cl 2p XPS spectra of the MFe_2O_4 catalysts after 10 h of chronopotentiometric electrolysis at 0.5 A·cm^{-2} in alkalized seawater. (b) Quantitative comparison of hypochlorite (ClO^-) yield for the four MFe_2O_4 samples, measured by iodometric potentiometric titration. (c) Correlation between ClO^- yield and M_{10000} of the four MFe_2O_4 catalysts.

are electron-rich species and thus compete for these metal cation active sites: spinel ferrites with strong *OH binding strength (e.g., $CoFe_2O_4$) have higher affinity for OH^- on their active sites, where OH^- occupies most sites and inhibits Cl^- adsorption. In contrast, those with weak *OH binding strength (e.g., $ZnFe_2O_4$) fail to adsorb OH^- effectively, leaving more active sites available for Cl^- and increasing its adsorption. Significantly, Cl^- adsorption is negatively correlated with sample magnetization (M_{10000}): stronger ferromagnetism corresponds to lower Cl^- adsorption, and vice versa. This is because strong ferromagnetism promotes spin alignment and enhances metal–oxygen hybridization, strengthening *OH binding and weakening the affinity of active sites for Cl^- to achieve dual regulation.

On the basis of Cl^- adsorption analysis, iodometric potentiometric titration [3, 15, 42] was employed to quantitatively determine the content of hypochlorite (ClO^-), the by-product generated by ClOR (Fig. S11 in the ESM). The titration principle is based on the oxidation-reduction reaction between ClO^- and I^- in an acidic environment ($ClO^- + 2I^- + 2H^+ = Cl^- + I_2 + H_2O$), and the content of ClO^- is calculated by the consumption of standard sodium thiosulfate solution ($I_2 + 2S_2O_3^{2-} = 2I^- + S_4O_6^{2-}$). The quantitative results of ClO^- are shown in Fig. 3(b), where the ClO^- yield follows the same trend as Cl^- adsorption, i.e., $CoFe_2O_4$ < $NiFe_2O_4$ < $MgFe_2O_4$ < $ZnFe_2O_4$. Specifically, the ClO^- yield of $CoFe_2O_4$ is the lowest (only 3.6 μmol), while $ZnFe_2O_4$ generates the highest ClO^- (16.8 μmol)—approximately 4.7 times that of $CoFe_2O_4$. Importantly, the ClO^- yield is negatively correlated with the magnetic strength of the samples, indicating an inherent correlation between them (Fig. 3(c)).

2.4 Key role of magnetism in inhibiting chlorine-related side reactions

As previously demonstrated, a negative correlation exists between catalyst magnetism and the yield of chlorine by-products (e.g., ClO^-), underscoring the critical role of magnetism in inhibiting chlorine-related side reactions and regulating the anodic selectivity of seawater electrolysis. To gain deeper insight into the underlying mechanism, the molecular orbital characteristics of key species involved in anodic reactions—OH^-, O_2, and Cl_2—were systematically investigated (Figs. 4(a)–4(c)). Specifically, OH^- and Cl_2 are singlet species with all electrons paired in their molecular orbitals, whereas O_2 exists in a triplet ground state, featuring two parallel unpaired electrons in its π* orbitals [18, 27]. This spin characteristic difference is the key premise for magnetism to regulate reaction selectivity, as it leads to distinct spin dependencies between OER and ClOR: OER is spin-nonconservative, requiring spin polarization to convert from OH^- to triplet O_2 ($4OH^- \rightarrow O_2 + 2H_2O + 4e^-$), while Cl_2 formation ($2Cl^- \rightarrow Cl_2 + 2e^-$) and subsequent conversion to ClO^- ($Cl_2 + 2OH^- \rightarrow ClO^- + Cl^- + H_2O$) are spin-independent, involving only singlet species without the need for spin selection.

The core mechanism by which magnetism inhibits chlorine-related side reactions lies in its regulation of spin alignment on the catalyst surface, which exerts opposite effects on the formation of chlorine products and O_2. Previous studies [21, 32] have shown that catalysts with aligned spins (e.g., ferromagnetic or chiral catalysts) can promote triplet O_2 formation by selecting electrons with appropriate spin orientations; conversely, catalysts with anti-aligned spins tend to generate oxygen intermediates with opposite spins, requiring an additional spin flip process to form triplet O_2 from OH^- (Fig. 4(d)). In sharp contrast, the formation of Cl_2 (the primary chlorine product) follows a distinct pathway (Fig. 4(e)): It requires the combination of two chlorine intermediates with opposite spins to achieve electron pairing in its molecular orbitals [18]. This combination process does not require spin selection; instead, the intermediates with parallel spins induced by spin alignment may be energetically unfavorable for the formation of the singlet product [18, 22, 34]. This can explain the observed negative correlation between catalyst magnetism and chlorine product yield: stronger magnetism may lead to more ordered spin alignment, which further enhances the inhibition of chlorine by-products and optimizes the selectivity of seawater electrolysis toward OER against chlorine-related side reactions.

To experimentally verify the above mechanism and further highlight the regulatory effect of magnetism on reaction selectivity, seawater electrolysis tests were conducted under an external magnetic field of 10,000 Oe (Fig. S12 in the ESM). Specifically, the magnetocurrent density (i.e., the difference in current density with and without an external magnetic field) revealed that ferromagnetic/ferrimagnetic spinel ferrites ($CoFe_2O_4$, $NiFe_2O_4$, $MgFe_2O_4$)—which exhibit intrinsic magnetic order—all displayed significantly enhanced current density under magnetic field stimulation (Fig. 4(f)). Note that the slight increase in current density of non-magnetic $ZnFe_2O_4$ was instead attributed to its growth on a magnetic Ni substrate, which indirectly induced a weak magnetic response [43]. This is further confirmed by the tests of loading the four catalysts onto non-magnetic carbon paper (Fig. S13 in the ESM). Additionally, the magnetocurrent (defined as [(current density with an external magnetic field − current density without an external magnetic field)/current density without an external magnetic field] × 100%) was positively correlated with the magnetic strength (M_{10000}) of the catalysts (Fig. 4(g)), which is consistent with previous reports [30]. This phenomenon stems from the external magnetic field, which further facilitates spin alignment among different magnetic domains, thereby enhancing OER efficiency through the spin selection effect.

More importantly, to quantitatively confirm the inhibitory effect of spin/magnetism on chlorine-related side reactions, $CoFe_2O_4$ was selected as the representative catalyst (owing to its strongest magnetic response) and subjected to detailed quantification of chlorine by-products under external magnetic field conditions (Fig. 4(h) and Fig. S14 in the ESM). At an applied potential of 1.85 V versus reversible hydrogen electrode (vs. RHE), the application of an external magnetic field led to a significant decrease in ClO^- yield, dropping from 2.6 to 1.3 μmol (a 50% reduction). Furthermore, the proportion of charge consumed for ClO^- generation relative to the total charge passed (Q_{ClO^-}/Q_{total})—a key indicator of chlorine-related side reaction severity—decreased more drastically, corresponding to a relative decrease of approximately 53.7%. This significant reduction clearly demonstrates that spin/magnetic effects can effectively inhibit the formation of chlorine by-products while simultaneously enhancing OER efficiency, thereby substantially improving the anodic selectivity of seawater electrolysis. Consistent with previous reports [22, 34] on spin-dependent suppression of singlet H_2O_2 (a singlet reactive oxygen species) via spin alignment, the magnetism-induced spin order in this work specifically targets singlet chlorine species, further validating the specificity and efficacy of spin control in side reaction regulation.

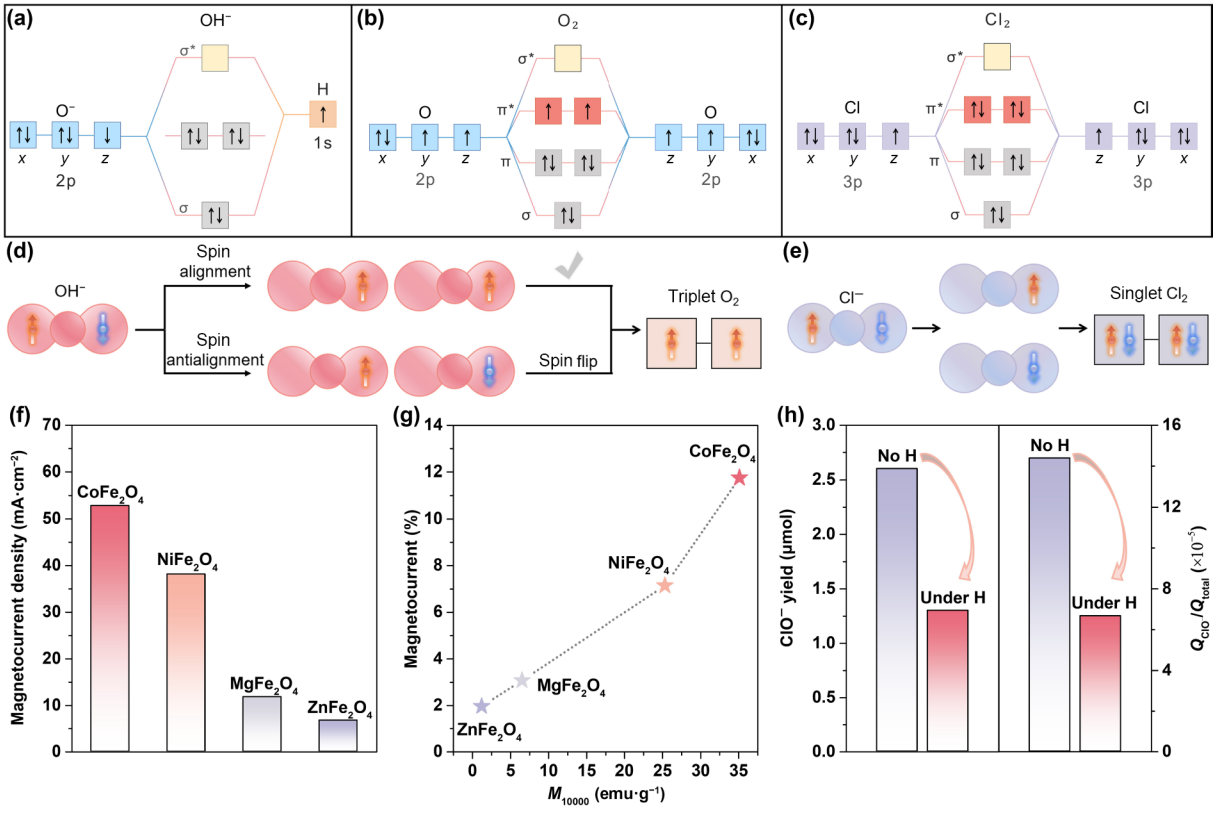

Figure 4 Spin control over chlorine-related side reaction and mechanism verification. (a)–(c) Molecular orbital diagrams of OH^-, O_2, and Cl_2, respectively. (d) Schematic illustration of spin-dependent triplet O_2 formation during OER. (e) Schematic illustration of spin-independent singlet Cl_2 formation. (f) Magnetocurrent density of the MFe_2O_4 catalysts in alkalized seawater. (g) Correlation between the magnetocurrent and M_{10000} of the four catalysts. (h) Comparison of ClO^- yield and Q_{ClO^-}/Q_{total} for $CoFe_2O_4$ with and without an external magnetic field.

2.5 Stability evaluation of spinel ferrites in seawater electrolysis

The effective inhibition of chlorine side reactions by spin control not only optimizes anodic selectivity but also reduces the accumulation of corrosive chlorine species (e.g., ClO^-, Cl_2)—a factor critical for the long-term durability of seawater electrolysis. These chlorine species corrode catalyst active sites, damage electrolyzer components, and even shorten the service life of the entire electrolysis device [4, 44]; thus, spin alignment-regulated suppression of chlorine side reactions essentially reduces corrosive hazards, paving the way for stable practical seawater electrolysis.

To comprehensively evaluate the long-term durability of spinel ferrites with different magnetic properties in seawater electrolysis, durability tests were performed on the four spinel ferrite catalysts at a constant current density of 0.5 A·cm^{-2} for 200 h (Fig. 5(a)). The variation in applied potential during the electrolysis process was used to reflect catalyst durability, as an increase in potential typically indicates catalyst degradation. The results showed that the potential increase amplitude (ΔE) of the four catalysts followed the order: $CoFe_2O_4$ < $NiFe_2O_4$ < $MgFe_2O_4$ < $ZnFe_2O_4$ (Fig. 5(b)), consistent with the previously observed ClO^- yield trend. Corrosion potential measurements further supported this point (Fig. S15 in the ESM), with the sequence of $CoFe_2O_4$ > $NiFe_2O_4$ > $MgFe_2O_4$ > $ZnFe_2O_4$ (a more positive potential indicates better corrosion resistance). Together, these results confirm that the magnetic properties of spinel ferrites regulate their corrosion resistance and long-term durability via spin control-induced inhibition of chlorine-related side reactions: stronger magnetism enhances chlorine suppression, reduces chlorine corrosion and catalyst degradation, and thus improves durability.

To further validate the practical application potential of strong magnetic spinel ferrites in seawater electrolysis, $CoFe_2O_4$—characterized by the strongest ferromagnetism, optimal selectivity, and superior durability—was employed as the anode catalyst to assemble an AEMWE for alkalized seawater electrolysis (Fig. 5(d) inset). Electrolyzer performance measurements revealed that the cell voltage was 1.84 V at a current density of 0.5 A·cm^{-2} and 2.10 V at 1.0 A·cm^{-2} (Fig. 5(c)), demonstrating excellent electrolysis efficiency. More importantly, the AEMWE achieved stable operation for 120 h under a constant current density of 0.5 A·cm^{-2}, with no significant increase in celwasl voltage or catalyst performance degradation (Fig. 5(d)). This finding fully validates the considerable application potential of strong magnetic catalysts in practical seawater electrolysis, offering a viable strategy for the development of high-efficiency and durable seawater electrolysis catalysts.

3 Conclusions

In summary, this work demonstrates that spin regulation in magnetic spinel oxides enables the selective modulation of adsorption affinities toward OH^-/Cl^-; the ferromagnetic effect promotes favorable spin alignment to facilitate the generation of triplet oxygen while impeding the formation of chlorine-containing byproducts. Benefiting from such well-regulated adsorption behavior and spin-dependent reaction pathways, catalysts with stronger ferromagnetism exhibit significantly suppressed chlorine-

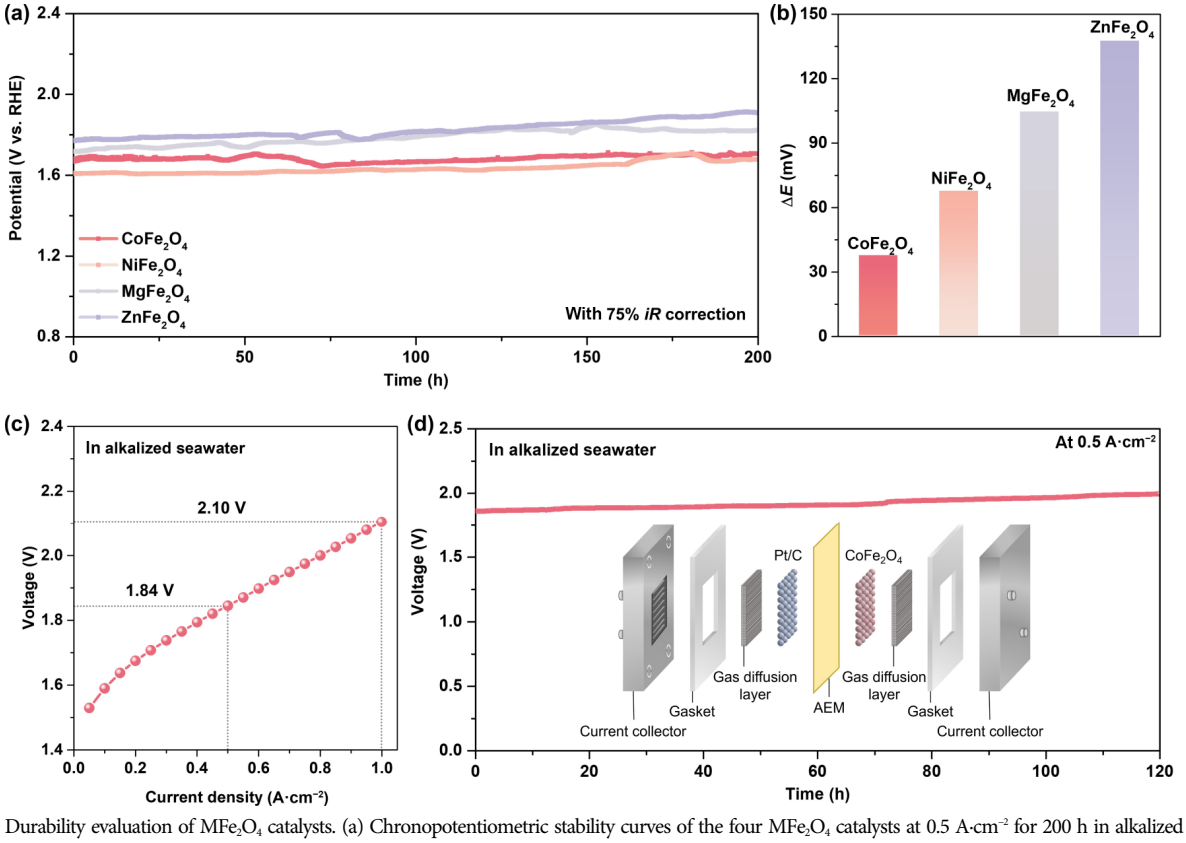

Figure 5 Durability evaluation of MFe_2O_4 catalysts. (a) Chronopotentiometric stability curves of the four MFe_2O_4 catalysts at 0.5 A·cm^{-2} for 200 h in alkalized seawater. (b) Comparison of the potential increase amplitude (ΔE) after stability test for the four MFe_2O_4 catalysts. (c) Polarization curve of the AEMWE using $CoFe_2O_4$ as the anode catalyst in alkalized seawater at 60 °C. (d) Long-term durability curve of the AEMWE at 0.5 A·cm^{-2} in alkalized seawater; inset: schematic diagram of the AEMWE device.

related side reactions and substantially enhanced operational stability for seawater electrolysis. Moreover, this spin-control strategy can be further extended to the rational design of non-noble electrocatalysts with intrinsic magnetism or chirality, providing a promising route for developing efficient, selective, and durable systems for large-scale seawater electrolysis and other spin-dependent electrochemical processes.

4 Experimental

4.1 Materials synthesis

$CoFe_2O_4$, $NiFe_2O_4$, $MgFe_2O_4$, and $ZnFe_2O_4$ were synthesized via a typical hydrothermal method [45]. For the synthesis of $CoFe_2O_4$, 0.375 mmol of $Co(NO_3)_2{\cdot}6H_2O$, 0.75 mmol of $Fe(NO_3)_3{\cdot}9H_2O$, 0.19 mmol of $C_6H_5O_7Na_3{\cdot}2H_2O$, 3.3 mmol of urea, and 1.0 mmol of polyacrylamide (PAM) were dispersed in 30 mL of deionized (DI) water and stirred vigorously for 60 min to form a homogeneous dispersion. The homogeneous solution was then transferred into a 50 mL Teflon-lined stainless-steel autoclave, which was heated at 200 °C for 12 h. After being cooled to room temperature, the resulting solid product was collected by centrifugation, washed repeatedly with DI water and ethanol to eliminate residual impurities, and finally dried in an oven at 60 °C for 12 h. $NiFe_2O_4$, $MgFe_2O_4$, and $ZnFe_2O_4$ were synthesized using the same procedure as $CoFe_2O_4$, except that $Co(NO_3)_2{\cdot}6H_2O$ was substituted with stoichiometric amounts of $Ni(NO_3)_2{\cdot}6H_2O$, $Mg(NO_3)_2{\cdot}6H_2O$, and $Zn(NO_3)_2{\cdot}6H_2O$, respectively.

4.2 Materials characterization

XRD patterns were recorded on a Bruker D8 Advance diffractometer with Cu Kα radiation over a 2θ range of 10°–80°. Magnetic properties of the synthesized spinel ferrites were characterized using a quantum design physical property measurement system (PPMS) at room temperature, and magnetic hysteresis loops were recorded in magnetic fields between −30,000 and +30,000 Oe. XPS measurements were performed on a Thermo Fisher Scientific Kα spectrometer with Al Kα radiation.

4.3 Hypochlorite quantification

Hypochlorite (ClO^-) yield was quantified by iodometric potentiometric titration. First, the electrolyte after continuous operation was collected, adjusted to pH 2–3 with H_2SO_4, and then mixed with excess freshly-prepared 0.5 M KI solution. A yellow color indicated the presence of ClO^-, as I^- was oxidized to I_2. The resulting I_2 was finally titrated with 0.02 M $Na_2S_2O_3$ solution, and the volume of consumed $Na_2S_2O_3$ solution was recorded.

The molar amount of ClO^- was calculated using the equation

$$n_{ClO^-} = C \times V/2 \quad (1)$$

where C (0.02 M) and V are the concentration and consumed volume of $Na_2S_2O_3$ solution, respectively. Subsequently, this value was scaled to the total electrolyte volume. The ClO^--associated charge (Q_{ClO^-}) was then calculated as

$$Q_{ClO^-} = n_{ClO^-} \times F \times 2 \quad (2)$$

where F is the Faraday constant and 2 represents the number of electrons per ClO^- species. This value was divided by the total charge (Q_{total}) passed during the stability test to obtain the radio of charge associated with the formation of ClO^- species.

4.4 Electrochemical measurements

All electrochemical measurements were performed on a CHI 660E electrochemical workstation (CH Instruments, Inc.) in a standard three-electrode system at room temperature. NF with *in-situ* grown catalyst was directly used as the working electrode, a graphite rod as the counter electrode, and a saturated calomel electrode (SCE) as the reference electrode. All potentials reported in this work were calibrated to the RHE scale [46].

Prior to catalyst growth, the NF substrate was sequentially pretreated with HNO_3 solution, DI water, and ethanol by ultrasonication to remove surface oxides and impurities. The working electrodes were directly fabricated through the hydrothermal synthesis process described above, where the target spinel ferrite catalysts were grown *in-situ* on the pre-cleaned NF substrates.

Cyclic voltammetry (CV) measurements were performed at a scan rate of 50 $mV \cdot s^{-1}$ in alkalized seawater electrolyte to obtain stable electrochemical signals prior to subsequent tests. LSV curves were recorded at a scan rate of 5 $mV \cdot s^{-1}$ in the same alkalized seawater electrolyte, with 75% *iR* correction. Potentiodynamic polarization curves were recorded at a scan rate of 10 $mV \cdot s^{-1}$ to measure the corrosion potential of the catalysts in alkalized seawater.

For electrochemical tests under an external magnetic field, a tunable magnetic field perpendicular to the electrode surface was provided by a Hall Effect Test System (CH-100, with the magnetic field intensity controlled at 10,000 Oe. All other test parameters were kept identical to those used in tests without an external magnetic field.

4.5 Anion exchange membrane water electrolyzer assembly and testing

For the AEMWE, a commercial FAA-3-50 anion exchange membrane was pretreated prior to assembly: It was initially immersed in 1.0 M NaOH for 48 h, then transferred to fresh 1.0 M NaOH for an additional 24 h. After pretreatment, the membrane was thoroughly rinsed with DI water until the washing water reached neutral pH. The anode consisted of the *in-situ* grown spinel ferrite catalyst supported on nickel fibre felt (instead of nickel foam), while the cathode was fabricated by spraying commercial Pt/C onto the pretreated membrane using an ultrasonic spray coater. Additionally, the Pt/C cathode ink was prepared by dispersing 100 mg of Pt/C in 10 mL of isopropanol-DI water mixture (1:3, v/v) with 5 wt.% Nafion as a binder, followed by ultrasonication for 3 h at room temperature to form a homogeneous ink. Subsequently, the pretreated AEM, anode catalyst-loaded nickel fibre felt, cathode nickel fibre felt, and Teflon gaskets were assembled sequentially and tightened to 4.5 N·m using a torque wrench.

For AEMWE performance testing, alkalized seawater (1 M NaOH + seawater) was employed as the feed electrolyte, which was circulated at 200 $mL \cdot min^{-1}$ via a two-channel peristaltic pump. Meanwhile, the electrolyzer temperature was maintained at 60 °C by a temperature controller, with thermocouples inserted into the endplates for real-time monitoring. Prior to formal testing, the electrolyzer was pre-activated via chronopotentiometry at a current density range of 0.01–1.20 $A \cdot cm^{-2}$ (0.01 $A \cdot cm^{-2}$ step, 10 s holding time) to achieve stable electrochemical performance. After activation, polarization curves (without *iR* correction) were recorded at a current density range of 0.05–1.00 $A \cdot cm^{-2}$ (0.05 $A \cdot cm^{-2}$ step, 15 s holding time). Finally, long-term stability was evaluated by testing at a constant current density of 0.5 $A \cdot cm^{-2}$ for 120 h, with real-time recording of cell voltage.

Electronic Supplementary Material: Supplementary material (additional characterizations and electrochemical tests) is available in the online version of this article at https://doi.org/10.26599/NR.2026.94908738.

Data availability

All data needed to support the conclusions in the paper are presented in the manuscript and the Electronic Supplementary Material. Additional data related to this paper may be requested from the corresponding author upon request.

Acknowledgements

This work was supported by the National Natural Science Foundation of China (Nos. U23A2086 and 52071231).

Declaration of competing interest

All the contributing authors report no conflict of interests in this work.

Author contribution statement

J. S. L.: Methodology, investigation, formal analysis, writing – original draft. R. G. W., J. X. G., Q. L. W., Z. L., and R. Z. M.: Validation, formal analysis. T. L.: Conceptualization, supervision, funding acquisition, writing – review & editing.

Use of AI statement

None.

References

[1] Xie, H. P.; Zhao, Z. Y.; Liu, T.; Wu, Y. F.; Lan, C.; Jiang, W. C.; Zhu, L. Y.; Wang, Y. P.; Yang, D. S.; Shao, Z. P. A membrane-based seawater electrolyser for hydrogen generation. *Nature* **2022**, *612*, 673–678.

[2] Sha, Q. H.; Wang, S. Y.; Yan, L.; Feng, Y. S.; Zhang, Z.; Li, S. H.; Guo, X. L.; Li, T. S.; Li, H.; Zhuang, Z. B. et al. 10,000-h-stable intermittent alkaline seawater electrolysis. *Nature* **2025**, *639*, 360–367.

[3] Guo, J. X.; Zheng, Y.; Hu, Z. P.; Zheng, C. Y.; Mao, J.; Du, K.; Jaroniec, M.; Qiao, S. Z.; Ling, T. Direct seawater electrolysis by adjusting the local reaction environment of a catalyst. *Nat. Energy* **2023**, *8*, 264–272.

[4] Tong, W. M.; Forster, M.; Dionigi, F.; Dresp, S.; Sadeghi Erami, R.; Strasser, P.; Cowan, A. J.; Farràs, P. Electrolysis of low-grade and saline surface water. *Nat. Energy* **2020**, *5*, 367–377.

[5] Yu, L.; Ning, M. H.; Wang, Y.; Yuan, C. Q.; Ren, Z. F. Direct seawater electrolysis for hydrogen production. *Nat. Rev. Mater.* **2025**, *10*, 857–873.

[6] Chen, L.; Yu, C.; Dong, J. T.; Han, Y. N.; Huang, H. L.; Li, W. B.;

Zhang, Y. F.; Tan, X. Y.; Qiu, J. S. Seawater electrolysis for fuels and chemicals production: Fundamentals, achievements, and perspectives. *Chem. Soc. Rev.* **2024**, *53*, 7455–7488.

[7] Cai, Z. W.; Liang, J.; Li, Z. X.; Yan, T. Y.; Yang, C. X.; Sun, S. J.; Yue, M.; Liu, X. W.; Xie, T.; Wang, Y. et al. Stabilizing NiFe sites by high-dispersity of nanosized and anionic Cr species toward durable seawater oxidation. *Nat. Commun.* **2024**, *15*, 6624.

[8] Duan, X. X.; Sha, Q. H.; Li, P. S.; Li, T. S.; Yang, G. T.; Liu, W.; Yu, E. D.; Zhou, D. J.; Fang, J. J.; Chen, W. X. et al. Dynamic chloride ion adsorption on single iridium atom boosts seawater oxidation catalysis. *Nat. Commun.* **2024**, *15*, 1973.

[9] He, X.; Yao, Y. C.; Zhang, L. M.; Wang, H. F.; Tang, H.; Jiang, W. L.; Ren, Y. C.; Nan, J.; Luo, Y. S.; Wu, T. W. et al. Hexafluorophosphate additive enables durable seawater oxidation at ampere-level current density. *Nat. Commun.* **2025**, *16*, 4998.

[10] Sun, X. G.; Shen, W.; Liu, H.; Xi, P. X.; Jaroniec, M.; Zheng, Y.; Qiao, S. Z. Corrosion-resistant NiFe anode towards kilowatt-scale alkaline seawater electrolysis. *Nat. Commun.* **2024**, *15*, 10351.

[11] Liu, W.; Yu, J. G.; Li, T. S.; Li, S. H.; Ding, B. Y.; Guo, X. L.; Cao, A. Q.; Sha, Q. H.; Zhou, D. J.; Kuang, Y. et al. Self-protecting CoFeAl-layered double hydroxides enable stable and efficient brine oxidation at 2 $A \cdot cm^{-2}$. *Nat. Commun.* **2024**, *15*, 4712.

[12] Shen, W.; Ye, Y. Z.; Hu, Y.; Wu, H. Y.; Xia, Q. J.; Xie, H. D.; Li, Z. J.; Zhang, N.; An, L.; Si, R. et al. Corrosion protection of rare earth for kilowatt-level alkaline seawater electrolyzer. *J. Am. Chem. Soc.* **2025**, *147*, 17190–17200.

[13] Liu, W.; Yu, J. G.; Sendeku, M. G.; Li, T. S.; Gao, W. Q.; Yang, G. T.; Kuang, Y.; Sun, X. M. Ferricyanide armed anodes enable stable water oxidation in saturated saline water at 2 A/cm^2. *Angew. Chem., Int. Ed.* **2023**, *62*, e202309882.

[14] Xu, W. W.; Wang, Z. F.; Liu, P. Y.; Tang, X.; Zhang, S. X.; Chen, H. C.; Yang, Q. H.; Chen, X.; Tian, Z. Q.; Dai, S. et al. Ag nanoparticle-induced surface chloride immobilization strategy enables stable seawater electrolysis. *Adv. Mater.* **2024**, *36*, 2306062.

[15] Dionigi, F.; Reier, T.; Pawolek, Z.; Gliech, M.; Strasser, P. Design criteria, operating conditions, and nickel-iron hydroxide catalyst materials for selective seawater electrolysis. *ChemSusChem* **2016**, *9*, 962–972.

[16] Kuang, Y.; Kenney, M. J.; Meng, Y. T.; Hung, W. H.; Liu, Y. J.; Huang, J. E.; Prasanna, R.; Li, P. S.; Li, Y. P.; Wang, L. et al. Solar-driven, highly sustained splitting of seawater into hydrogen and oxygen fuels. *Proc. Natl. Acad. Sci. USA* **2019**, *116*, 6624–6629.

[17] Fan, R. L.; Liu, C. H.; Li, Z. H.; Huang, H. T.; Feng, J. Y.; Li, Z. S.; Zou, Z. G. Ultrastable electrocatalytic seawater splitting at ampere-level current density. *Nat. Sustain.* **2024**, *7*, 158–167.

[18] Liu, Y. D.; Li, L.; Li, X. N.; Xu, Y. F.; Wu, D. S.; Sakthivel, T.; Guo, Z. X.; Zhao, X. X.; Dai, Z. F. Asymmetric tacticity navigates the localized metal spin state for sustainable alkaline/sea water oxidation. *Sci. Adv.* **2025**, *11*, eads0861.

[19] Yu, Y.; Zhou, W.; Yuan, J. S.; Zhou, X. H.; Meng, X. X.; Zhang, X. W.; Li, X. H.; Xue, N. Y.; Chen, Y. J.; Xia, X. et al. A hydrogen-bond network sieve enables selective OH^-/Cl^- discrimination for stable seawater splitting at 2.0 $A \cdot cm^{-2}$. *Energy Environ. Sci.* **2025**, *18*, 9949–9958.

[20] Gracia, J. Spin dependent interactions catalyse the oxygen electrochemistry. *Phys. Chem. Chem. Phys.* **2017**, *19*, 20451–20456.

[21] Sang, Y. T.; Tassinari, F.; Santra, K.; Zhang, W. Y.; Fontanesi, C.; Bloom, B. P.; Waldeck, D. H.; Fransson, J.; Naaman, R. Chirality enhances oxygen reduction. *Proc. Natl. Acad. Sci. USA* **2022**, *119*, e2202650119.

[22] Mtangi, W.; Tassinari, F.; Vankayala, K.; Vargas Jentzsch, A.; Adelizzi, B.; Palmans, A. R. A.; Fontanesi, C.; Meijer, E. W.; Naaman, R. Control of electrons' spin eliminates hydrogen peroxide formation during water splitting. *J. Am. Chem. Soc.* **2017**, *139*, 2794–2798.

[23] Li, J. S.; Zheng, C. Y.; Zhao, E. L.; Mao, J.; Cheng, Y. H.; Liu, H.; Hu, Z. P.; Ling, T. Ferromagnetic ordering correlated strong metal-oxygen hybridization for superior oxygen reduction reaction activity. *Proc. Natl. Acad. Sci. USA* **2023**, *120*, e2307901120.

[24] Li, J. S.; Zhao, E. L.; Zhao, Y.; Wang, R. G.; Guo, J. X.; Wang, Q. L.; Mao, J.; Ling, T. A molecular catalyst-like oxide with strong redox capability for electrocatalysis. *Chem. Mater.* **2025**, *37*, 1027–1036.

[25] Jiao, Y. Z.; Sharpe, R.; Lim, T.; Niemantsverdriet, J. W. H.; Gracia, J. Photosystem II acts as a spin-controlled electron gate during oxygen formation and evolution. *J. Am. Chem. Soc.* **2017**, *139*, 16604–16608.

[26] Sun, Y. M.; Sun, S. N.; Yang, H. T.; Xi, S. B.; Gracia, J.; Xu, Z. J. Spin-related electron transfer and orbital interactions in oxygen electrocatalysis. *Adv. Mater.* **2020**, *32*, 2003297.

[27] Li, J. S.; Ma, J. J.; Ma, Z. A.; Zhao, E. L.; Du, K.; Guo, J. X.; Ling, T. Spin effect on oxygen electrocatalysis. *Adv. Energy Sustain. Res.* **2021**, *2*, 2100034.

[28] Ren, X.; Wu, T. Z.; Sun, Y. M.; Li, Y.; Xian, G. Y.; Liu, X. H.; Shen, C. M.; Gracia, J.; Gao, H. J.; Yang, H. T. et al. Spin-polarized oxygen evolution reaction under magnetic field. *Nat. Commun.* **2021**, *12*, 2608.

[29] Liang, Y. C.; Banjac, K.; Martin, K.; Zigon, N.; Lee, S.; Vanthuyne, N.; Garcés-Pineda, F. A.; Galán-Mascarós, J. R.; Hu, X. L.; Avarvari, N. et al. Enhancement of electrocatalytic oxygen evolution by chiral molecular functionalization of hybrid 2D electrodes. *Nat. Commun.* **2022**, *13*, 3356.

[30] Garcés-Pineda, F. A.; Blasco-Ahicart, M.; Nieto-Castro, D.; López, N.; Galán-Mascarós, J. R. Direct magnetic enhancement of electrocatalytic water oxidation in alkaline media. *Nat. Energy* **2019**, *4*, 519–525.

[31] Hunt, C.; Zhang, Z. S.; Ocean, K.; Jansonius, R. P.; Abbas, M.; Dvorak, D. J.; Kurimoto, A.; Lees, E. W.; Ghosh, S.; Turkiewicz, A. et al. Quantification of the effect of an external magnetic field on water oxidation with cobalt oxide anodes. *J. Am. Chem. Soc.* **2022**, *144*, 733–739.

[32] Wu, T. Z.; Ren, X.; Sun, Y. M.; Sun, S. N.; Xian, G. Y.; Scherer, G. G.; Fisher, A. C.; Mandler, D.; Ager, J. W.; Grimaud, A. et al. Spin pinning effect to reconstructed oxyhydroxide layer on ferromagnetic oxides for enhanced water oxidation. *Nat. Commun.* **2021**, *12*, 3634.

[33] Sun, Z. M.; Lin, L.; He, J. L.; Ding, D. J.; Wang, T. Y.; Li, J.; Li, M. X.; Liu, Y. C.; Li, Y. Y.; Yuan, M. W. et al. Regulating the spin state of Fe^{III} enhances the magnetic effect of the molecular catalysis mechanism. *J. Am. Chem. Soc.* **2022**, *144*, 8204–8213.

[34] Zhang, W. Y.; Banerjee-Ghosh, K.; Tassinari, F.; Naaman, R. Enhanced electrochemical water splitting with chiral molecule-coated Fe_3O_4 nanoparticles. *ACS Energy Lett.* **2018**, *3*, 2308–2313.

[35] Zhou, Y.; Sun, S. N.; Xi, S. B.; Duan, Y.; Sritharan, T.; Du, Y. H.; Xu, Z. J. Superexchange effects on oxygen reduction activity of edge-sharing $[Co_xMn_{1-x}O_6]$ octahedra in spinel oxide. *Adv. Mater.* **2018**, *30*, 1705407.

[36] Wei, C.; Feng, Z. X.; Scherer, G. G.; Barber, J.; Shao-Horn, Y.; Xu, Z. J. Cations in octahedral sites: A descriptor for oxygen electrocatalysis on transition-metal spinels. *Adv. Mater.* **2017**, *29*, 1606800.

[37] Gracia, J.; Sharpe, R.; Munarriz, J. Principles determining the activity of magnetic oxides for electron transfer reactions. *J. Catal.* **2018**, *361*, 331–338.

[38] Suntivich, J.; May, K. J.; Gasteiger, H. A.; Goodenough, J. B.; Shao-Horn, Y. A perovskite oxide optimized for oxygen evolution catalysis from molecular orbital principles. *Science* **2011**, *334*, 1383–1385.

[39] Suntivich, J.; Gasteiger, H. A.; Yabuuchi, N.; Nakanishi, H.; Goodenough, J. B.; Shao-Horn, Y. Design principles for oxygen-reduction activity on perovskite oxide catalysts for fuel cells and metal-air batteries. *Nat. Chem.* **2011**, *3*, 546–550.

[40] Hwang, J.; Rao, R. R.; Giordano, L.; Katayama, Y.; Yu, Y.; Shao-Horn, Y. Perovskites in catalysis and electrocatalysis. *Science* **2017**, *358*, 751–756.

[41] Tao, H. B.; Xu, Y. H.; Huang, X.; Chen, J. Z.; Pei, L. J.; Zhang, J. M.; Chen, J. G.; Liu, B. A general method to probe oxygen evolution intermediates at operating conditions. *Joule* **2019**, *3*, 1498–1509.

[42] Qi, M. H.; Qin, M. K.; Wang, H.; Lin, B. B.; Chen, J. D.; Shi, X. Y.; Du, X. B. W.; Mao, S. J.; Zhao, J. P.; Zhang, H. et al. Regulating the redox cycle of nickel species for efficient seawater electrolysis. *Appl. Catal. B: Environ. Energy* **2024**, *356*, 124259.

[43] Ge, J. J.; Chen, R. R.; Ren, X.; Liu, J. W.; Ong, S. J. H.; Xu, Z. J. Ferromagnetic-antiferromagnetic coupling core–shell nanoparticles with spin conservation for water oxidation. *Adv. Mater.* **2021**, *33*, 2101091.

[44] Zhang, S. X.; Xu, W. W.; Chen, H. C.; Yang, Q. H.; Liu, H.; Bao, S. J.; Tian, Z. Q.; Slavcheva, E.; Lu, Z. Y. Progress in anode stability improvement for seawater electrolysis to produce hydrogen. *Adv. Mater.* **2024**, *36*, 2311322.

[45] Sun, J.; Xue, H.; Zhang, Y. F.; Zhang, X. L.; Guo, N. K.; Song, T. S.; Dong, H. L.; Kong, Y.; Zhang, J. W.; Wang, Q. Unraveling the synergistic effect of heteroatomic substitution and vacancy engineering in $CoFe_2O_4$ for superior electrocatalysis performance. *Nano Lett.* **2022**, *22*, 3503–3511.

[46] Liang, Y. Y.; Li, Y. G.; Wang, H. L.; Zhou, J. G.; Wang, J.; Regier, T.; Dai, H. J. Co_3O_4 nanocrystals on graphene as a synergistic catalyst for oxygen reduction reaction. *Nat. Mater.* **2011**, *10*, 780–786.